International Journal of Microwave and Wireless Technologies, 2016, 8(3), 603–613.
doi:10.1017/S1759078715000343

RESEARCH PAPER

Stationary planar-surface target detection in an unknown indoor environment

HONGHUI YAN[1], QIAOZHEN LIU[2] AND REINER S. THOMÄ[1]

It is difficult to detect a stationary object in practice, especially in an unknown indoor environment, because (a) there is no distinct speed difference between the targets and the background; (b) responses of the targets are contaminated by dense unknown clutter; (c) a priori knowledge of the background is not always available for some scenarios. In this paper, a set of ultra-wideband sensors are used to detect a stationary target with a planar diffuse surface. It is shown that, the relative spectrum-shifts of the data after data-projection operation, are closely connected to the illumination-angle differences. Based on this, a detector is designed, and the location and the orientation of the target are determined. In order to mitigate the influence of clutters, a "time-shift & accumulation" scheme is designed to enhance the signal. As a consequence, the signal-to-interference-and-noise ratio is increased. In addition, results from measurement in a realistic indoor environment are provided.

Keywords: Radar signal processing and system modeling, Radar applications, Stationary target detection

Received 8 September 2014; Revised 2 February 2015; Accepted 5 February 2015; first published online 25 March 2015

I. INTRODUCTION

Indoor stationary object detection in an unknown environment is important for many civilian and military applications, such as indoor surveillance, search and rescue operations, logistics, security, and so on. However, it is challenging as compared with moving target detection, or target detection in a known environment, due to the highly cluttered indoor environment, the motionless nature of the targets concerned, as well as the lack of *a priori* information of the background for some scenarios (e.g. a disaster scenario after earthquake).

The detection of radar targets against a background of unwanted clutter due to echoes from the environment is a problem of fundamental interest in radar community [1]. Generally, the detection algorithm is designed based on the differences (or deviations) between the targets and the background (clutter, noise). The ability to distinguish objects depends on how much their properties (e.g. electromagnetic properties, motion properties, polarization, etc.) deviate from the properties of the background. Since the targets concerned are stationary objects, there would be no distinct speed difference between the targets and the background. Hence, it prevents the application of the motion-parameter-based detection techniques, e.g. Doppler-based approaches, subtraction (or cancellation) between sequence snapshots (e.g. Displaced Phased Center Antenna (DPCA)-based detection), etc. [1].

[1]Electronic Measurement Research Lab, Institute for Information Technology, Ilmenau University of Technology, Ilmenau 98693, Germany
[2]Beijing Institute of Astronautical Systems Engineering, Beijing 100076, China
Corresponding author:
H. Yan
Email: H.Yan@outlook.com

In literature, for the detection of a stationary object, background subtraction-related techniques are widely used to reduce the influence of background clutters (e.g. [2, 3]). Generally, it is assumed that "*a priori*" information about the environment can be acquired before presence of the target, and the target signature is contained in the residual of the subtraction operation. In literature [2, 4], after background subtraction, a computational time reversal (TR) technique is adopted to extract target information. Typically, it is realized by DORT (French acronym for "Decomposition of the Time Reversal Operator"), which relies on the assumption that the Green's function can be calculated (e.g. [5, 6]). However, under a layered medium condition (e.g. an indoor environment with walls), the computational TR demands a mathematical model of wall, in which the parameters of wall, such as thickness and real dielectric constant are required for construction of the mathematical model. In a realistic unknown indoor detection scenario, it is impractical to know all these detailed physical parameters of wall in advance.

Consider a stationary object detection scenario in an unknown realistic indoor environment (e.g. an indoor environment after disaster). Firstly, "*a priori*" information of the disaster environment is not always available in advance, so that it is not possible to use "background subtraction" related techniques any more. Extremely, for this unknown environment, the statistical distributions of clutter and noise are probably also unknown. This would even lead to difficulties in designing of a detector in the sense of statistics. Secondly, in indoor environments, targets (objects of interest) are typically surrounded by clutter (objects of uninterest). The responses of targets are not always stronger than that of clutter. It implies that we cannot always guarantee the signal-to-interference-and-noise ratio (SINR) of the system

is high enough so that the target can be detected. Thirdly, in indoor environments, there exists a number of objects and obstacles (e.g. wall) with unknown parameters. Owing to lack of parameter information of these obstacles, the Green's function is difficult to be constructed. This would further hinder the application of computational TR-related techniques.

In this paper, the concerned target is an object with a diffuse planar-surface. It can be testified that, for this kind of target, the reflections in different directions are angular-dependent, and with certain relationships among them. This property could be used to distinguish the target from other objects (clutter) in the environment. In fact, here, angular-dependent information is utilized, which has no relationship with the excess time-delay, incurred by obstacles such as walls. Therefore, it does not demand the knowledge of the obstacle parameters. In addition, in order to get a more reliable detection, a signal enhancement scheme is designed to enhance the signal. The byproduct of this operation is that the responses of clutter scattered from various sources (e.g. different objects in the surrounding) are non-uniformly time-shifted and accumulated. According to the Central Limit Theorem (CLT) of probability theory, the accumulation of clutter from a large number of different sources would approach Gaussian distribution. Thus, unknown clutter and noise are transformed into Gaussian clutter and noise. Correspondingly, a detector could be designed.

II. PROBLEM STATEMENT AND THE SIGNAL MODEL

We assume that the detection takes place in an unknown cluttered indoor environment, which is not possible to be probed before presence of the target. As an example, it may be an indoor environment after disaster. There are a number of objects and obstacles (e.g. wall) existing in the surroundings. The statistical distribution of clutter and noise is unknown.

We assume for our investigations that the target to be detected is an extended object with a planar-surface, on which there are a number of scatterers diffusing probing signals. As shown in Fig. 1, a set of ultra-wideband (UWB) radar sensors is used to detect the target. It consists of a number of receivers $R_m \in \{R_1,\ldots,R_M\}$, and one or more transmitters which move along predefined linear tracks $\mathbf{L}_l \in \{\mathbf{L}_1,\ldots,\mathbf{L}_L\}$, on which signals are transmitted at different transmission positions $T_n \in \{T_1,\ldots,T_N\}$. The environment is explored in a "*line by line*" manner by the movement of the transmitter. In order to improve the efficiency of the detection, several transmitters may be used to search several lines at the same time. In this way, a multiple-input multiple-output (MIMO) configuration is constructed.

Suppose $p(t)$ is the radiated waveform. Then, the signal received at the receiver R_m with respect to the transmission position T_n can be expressed as

$$s_{Rm,Tn}(t) = \sum_i a_{R_m,O_i,T_n} p(t - t'_{R_m,O_i,T_n}) + \sum_j a_{R_m,C_j,T_n} p(t - t'_{R_m,C_j,T_n}) + n_{R_m,T_n}(t), \quad (1)$$

where i and j are the indexes of O_i and C_j. As shown in Fig. 1, O_i and C_j denote objects in and out of the line under exploration (e.g. $\mathbf{L}_l$), respectively. The first term of the right part of (1) is the response of the objects (e.g. O_i) in the line under exploration. The second term is the response of the objects (e.g. C_j) out of the line under exploration. $n_{R_m,T_n}(t)$ is additive noise. a_{R_m,O_i,T_n} and a_{R_m,C_j,T_n} are the complex reflectivities due to the interaction of the reflections from the scatterers located on the objects O_i and C_j, respectively. Their values depend on a number of factors, such as the orientation of object, the illumination geometry of transmitter–receiver pair "$R_m - T_n$", etc. For the scope of the paper, the antenna gain and the signal fading due to propagation are ignored hereinafter.

The parameter

$$t'_{R_m,O_i,T_n} = [|\mathbf{R}_m - \mathbf{O}_i| + |\mathbf{O}_i - \mathbf{T}_n|]/c,$$

where $\mathbf{R}_m$, $\mathbf{O}_i$, and $\mathbf{T}_n$ are, respectively, the position vectors of R_m, O_i and T_n, is the average time-delay of the signals scattered by the scatterers located on the object O_i. Subscript "R_m, O_i, T_n" is used to indicate the parameters associated with propagating path "$R_m \leftarrow O_i \leftarrow T_n$". Subscript "$R_m$, T_n" indicates the parameters related to the transmitter–receiver pair "$R_m - T_n$". The symbol $|\cdot|$ is a modulus operator, and c is

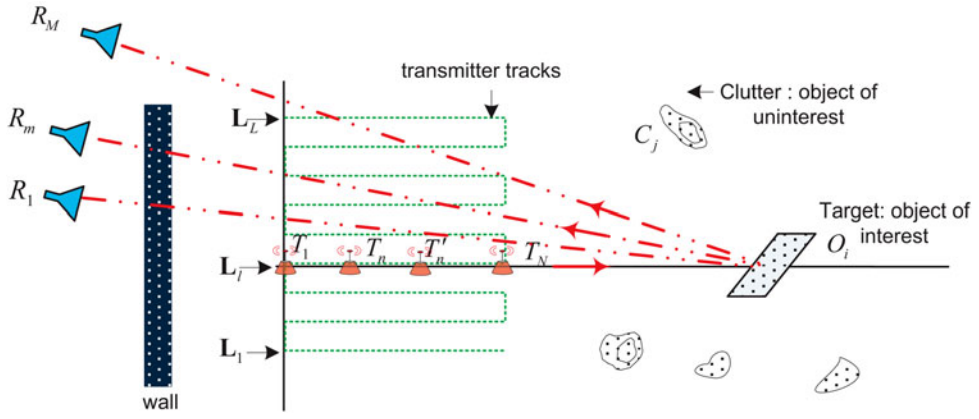

Fig. 1. Measurement configuration. The transmitter moves along predefined tracks. $T_1,\ldots,T_n,\ldots,T_N$ are different transmission positions on the track $\mathbf{L}_l$. "$R_1,\ldots,R_M$" are sparsely spaced receivers with different reception angles. It is noted that the walls in the scenario could appear anywhere, not just the location indicated in this figure.

https://doi.org/10.1017/S1759078715000343 Published online by Cambridge University Press

the wave propagation speed. Likewise

$$t'_{R_m,C_j,T_n} = [|\mathbf{R}_m - \mathbf{C}_j| + |\mathbf{C}_j - \mathbf{T}_n|]/c,$$

where $\mathbf{C}_j$ is the position vector of C_j, is the average time-delay with respect to the clutter C_j.

It should be noted that, for each detection, the responses of the objects out of the line under exploration, i.e. the second term of (1), will be regarded as *clutter*. Since the target is stationary, it is less practical to suppress the second term of (1) via motion-related techniques (e.g. subtraction or cancellation of sequence snapshots). Furthermore, because *a priori* information of the background is not available in our scenario, background subtraction-related techniques are not able to be used any more.

In addition, due to the fact that there exist plenty of objects in a typical indoor environment, for the data segment within a certain time slot of the received signal, it could be a mixture of responses scattered from objects situated on a certain ellipse (e.g. the ellipse shown in Fig. 1, or in three-dimensional (3D) case, an ellipsoid). This implies that the response of a target can probably be contaminated by responses of many other objects, which are located on the same ellipse with the target. In this case, we cannot always guarantee that the response of the target is strong enough to be detected.

Figure 2 gives the flowchart of our proposed algorithm. In order to get a reliable detection, it is necessary to enhance the signal before detection. For our concerned unknown environment, after the signal enhancement procedure, the statistical distribution of clutter could be changed into Gaussian distribution. Afterward, the detection is operated in a Gaussian clutter and noise environment using a kind of angular-dependent spectrum-shift information.

III. SIGNAL ENHANCEMENT

In (1), the value of a_{R_m,O_i,T_n} or a_{R_m,C_j,T_n} highly depends on the orientation of the target and the corresponding illumination geometry. However, for the same orientation of the target, $a_{R_m,O_i,T_n} = a_{R_m,O_i,T'_n}$ holds, under the condition

$$\frac{\mathbf{T}_n - \mathbf{O}_i}{|\mathbf{T}_n - \mathbf{O}_i|} = \frac{\mathbf{T}'_n - \mathbf{O}_i}{|\mathbf{T}'_n - \mathbf{O}_i|}, \tag{2}$$

where $\mathbf{T}_n$ and $\mathbf{T}'_n$ are the different transmission positions in the line under exploration, e.g. $\mathbf{L}_l$, as shown in Fig. 1. Under this condition, we can further have $|\mathbf{T}_n - \mathbf{O}_i| - |\mathbf{T}'_n - \mathbf{O}_i| = |\mathbf{T}_n - \mathbf{T}'_n|$.

Obviously, for the objects in the concerned line, $\mathbf{T}_n$ and $\mathbf{T}'_n$ have the same illumination angles. But for the objects out of this line, they have different illumination angles. Therefore, for the objects in the concerned line, the same distance between $\mathbf{T}_n$ and $\mathbf{T}'_n$ would induce the same time-delay difference given by

$$\begin{aligned} t^{diff}_{T_n,T'_n} &= t'_{R_m,O_i,T_n} - t'_{R_m,O_i,T'_n} \\ &= [|\mathbf{T}_n - \mathbf{O}_i| - |\mathbf{T}'_n - \mathbf{O}_i|]/c = |\mathbf{T}_n - \mathbf{T}'_n|/c. \end{aligned} \tag{3}$$

However, it would induce different time-delay differences for the objects out of this line, due to the fact that $|\mathbf{T}_n - \mathbf{C}_j| - |\mathbf{T}'_n - \mathbf{C}_j| \neq |\mathbf{T}_n - \mathbf{T}'_n|$.

According to (3), if taking the transmission position $\mathbf{T}_1$ as a reference, we have

$$p(t - t'_{R_m,O_i,T_n} + t^{diff}_{T_n,T_1}) = p(t - t'_{R_m,O_i,T_1}), \tag{4}$$

where the time-delay difference $t^{diff}_{T_n,T_1}$ only depends on the transmission positions. This implies that, for the objects located in the line under exploration, their time-delays with respect to different transmission positions could be compensated and then aligned by the operation given by (4).

Based on the signal model given by (1), let us consider a "*time-shift* & *accumulation*" operation which is described as

$$\begin{aligned} \sum_{n=1}^{N} s_{R_m,T_n}(t + t^{diff}_{T_n,T_1}) &= N \sum_i a_{R_m,O_i,T_n} p(t - t'_{R_m,O_i,T_1}) \\ &+ \sum_{n=1}^{N} \sum_j a_{R_m,C_j,T_n} p(t - t'_{R_m,C_j,T_n} + t^{diff}_{T_n,T_1}) \\ &+ \sum_{n=1}^{N} n_{R_m,T_n}(t + t^{diff}_{T_n,T_1}), \end{aligned} \tag{5}$$

where n is the index of the transmission positions. The first and second terms of the right part of the equation, are the accumulations of responses scattered from the objects located in and out of the line under exploration, respectively. The third term is noise. It is noted that

- in the line under exploration: the responses of the objects (O_i) are time-shifted, aligned and then accumulated. It is a coherent operation, where the parameter $t^{diff}_{T_n,T_1}$ is used for time-delay correction. Responses are enhanced for N times as compared with the case of single transmission data.
- Out of the line under exploration: the responses of objects (C_j) are non-uniformly time-shifted, disturbed, and then accumulated. It is an incoherent operation, because $a_{R_m,C_j,T_n} \neq a_{R_m,C_j,T'_n}$, and the fact that the parameter $t^{diff}_{T_n,T_1}$ could further disturb the arriving-time of the responses. As a consequence, for a certain time-slot, the responses from objects located on different ellipses (or ellipsoids) are non-uniformly time-shifted and accumulated. Hence, these responses are attenuated as compared with the output of the coherent operation above.

The main steps of the operation are summarized as follows:

(a) move the transmitter along a certain track, e.g. $\mathbf{L}_l$;
(b) execute the "time-shift & accumulation" operation to enhance the signal. In the operation, responses of objects located in $\mathbf{L}_l$ are aligned, whereas responses of objects out of $\mathbf{L}_l$ are non-uniformly time-shifted (disturbed);

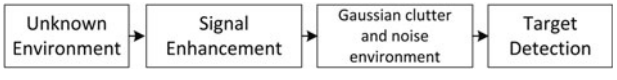

Fig. 2. Flow chart of the algorithm.

https://doi.org/10.1017/S1759078715000343 Published online by Cambridge University Press

(c) target detection along the track $\mathbf{L}_i$;
(d) repeat (a)–(c) for other tracks.

IV. DATA-PROJECTION AND THE SPECTRUM-SHIFT

A) Data-projection

As shown in Fig. 3, $\mathbf{X}$ is an arbitrarily scatterer located on the surface of the concerned target (e.g. O_i in Fig. 1). $\mathbf{X}_o$ denotes a reference point (e.g. the center of surface).

Owing to the existence of walls in the indoor environment, excess time-delay occurs when rays penetrate wall materials. Denote as $\zeta(\mathbf{B}, \mathbf{A})$ the excess time delay existing in the propagating path starting from point $\mathbf{A}$ and ending at point $\mathbf{B}$. Then, the propagation time between the transmitter $\mathbf{T}_n$, scatterer $\mathbf{X}$, and receiver $\mathbf{R}_i$ can be expressed as

$$t'(\mathbf{R}_i, \mathbf{X}, \mathbf{T}_n) = d(\mathbf{R}_i, \mathbf{X}, \mathbf{T}_n)/c + \zeta(\mathbf{R}_i, \mathbf{X}) + \zeta(\mathbf{X}, \mathbf{T}_n), \quad (6)$$

where $d(\mathbf{R}_i, \mathbf{X}, \mathbf{T}_n) = |\mathbf{R}_i - \mathbf{X}| + |\mathbf{T}_n - \mathbf{X}|$ is the range of propagation.

Suppose the target locates in the far field of the radar sensors, and the spatial extent is far less than its distance to the radar sensors. It is reasonable to assume that all the scatterers on the concerned extended target have the same excess time-delay. This implies that the excess time-delay does not change with the variation of scatterer's position $\mathbf{X}$. Mathematically, it can be assumed that

$$\frac{\partial}{\partial \mathbf{X}}[\zeta(\mathbf{R}_i, \mathbf{X}) + \zeta(\mathbf{X}, \mathbf{T}_n)] = 0.$$

Then (6) can be expanded at the nearby of $\mathbf{X}_o$ as

$$t'(\mathbf{R}_i, \mathbf{X}, \mathbf{T}_n) \approx t'(\mathbf{R}_i, \mathbf{X}_o, \mathbf{T}_n) + \tau. \quad (7)$$

The variable τ is the time-delay induced by the variation of scatterer positions,

$$\tau = \mathrm{grad}_x(d(\mathbf{R}_i, \mathbf{X}, \mathbf{T}_n))|_{\mathbf{X}=\mathbf{X}_o} \cdot \Delta\mathbf{X}/c = \mathbf{p}_{ref} \cdot \Delta\mathbf{X}, \quad (8)$$

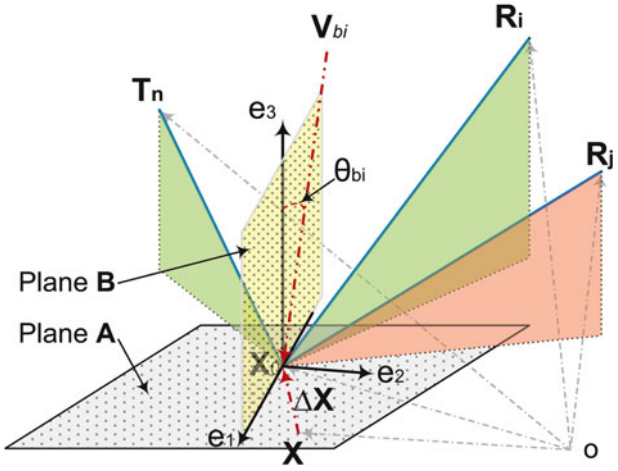

Fig. 3. Illumination geometry with respect to the target's surface plane.

where $\mathbf{p}_{ref} = \mathrm{grad}_x(d(\mathbf{R}_i, \mathbf{X}, \mathbf{T}_n))|_{\mathbf{X}=\mathbf{X}_o}/c$ is a reference vector selected. $\Delta\mathbf{X} = \mathbf{X} - \mathbf{X}_o$ is a vector on the target-surface plane. $\mathrm{grad}_x(\cdot)$ is a gradient operator with respect to the variable $\mathbf{X}$. According to the concept of gradient operation, $\mathrm{grad}_x(d(\mathbf{R}_i, \mathbf{X}, \mathbf{T}_n))$ points to the direction of the greatest rate of change of the distance $d(\mathbf{R}_i, \mathbf{X}, \mathbf{T}_n)$. It determines the direction of $\mathbf{p}_{ref}$. Here, "$\cdot$" is a dot-product operator. Via the dot-product operation given in (8), the vector $\Delta\mathbf{X}$ is projected onto the direction of the reference vector $\mathbf{p}_{ref}$.

Similarly, consider the time-delay of the signal received by R_j, whose reception angle is different from that of R_i. When projecting the data onto the same reference vector $\mathbf{p}_{ref}$, the time-delay can be given as

$$t'(\mathbf{R}_j, \mathbf{X}, \mathbf{T}_n) \approx t'(\mathbf{R}_i, \mathbf{X}_o, \mathbf{T}_n) + \gamma_{j,i}\tau, \quad (9)$$

where $\gamma_{j,i}$ is a scaling factor,

$$\gamma_{j,i} = \frac{\mathrm{grad}_x(d(\mathbf{R}_j, \mathbf{X}, \mathbf{T}_n))|_{\mathbf{X}=\mathbf{X}_o} \cdot \Delta\mathbf{X}}{\mathrm{grad}_x(d(\mathbf{R}_i, \mathbf{X}, \mathbf{T}_n))|_{\mathbf{X}=\mathbf{X}_o} \cdot \Delta\mathbf{X}} = 1 + \frac{(\mathbf{U}_{R_j,X_o} - \mathbf{U}_{R_i,X_o})}{\mathbf{V}_{bi} \cdot \Delta\mathbf{X}}. \quad (10)$$

In (10), $\mathbf{V}_{bi} = \mathbf{U}_{T_n,X_o} + \mathbf{U}_{R_i,X_o}$. $\mathbf{U}_{T_n,X_o}$ and $\mathbf{U}_{R_i,X_o}$ are the unit vectors of $\mathbf{T}_n - \mathbf{X}_o$, and $\mathbf{R}_i - \mathbf{X}_o$, respectively. $\mathbf{U}_{R_j,X_o}$ is the unit vector of $\mathbf{R}_j - \mathbf{X}_o$. It can be proven that $\mathbf{V}_{bi}$ locates on the bisector of the angle $\measuredangle R_i X_o T_n$.

In fact, (8)–(10) define a data-projection operation, in which, $\Delta\mathbf{X}$, the location variations of scatterers on the target-surface plane with respect to the different receivers R_i and R_j, are projected onto the same the reference vector $\mathbf{p}_{ref}$. In other words, the location variations $\Delta\mathbf{X}$ on the target-surface plane are translated into time-delay variations in the direction of the reference vector $\mathbf{p}_{ref}$. In the perspective of signal processing, it would correspond to a resampling operation, in which the resampling rate is controlled by the parameter $\gamma_{j,i}$.

Apparently, due to the existence of the scaling factor $\gamma_{j,i}$, even for the same location variation $\Delta\mathbf{X}$ on the target-surface plane, it will induce different time-delays, τ and $\gamma_{j,i}\tau$, with respect to different illumination geometries, e.g. "$\mathbf{T}_n \to \mathbf{X} \to \mathbf{R}_i$" and "$\mathbf{T}_n \to \mathbf{X} \to \mathbf{R}_j$". Consequently, it will further impact on the spectrum in frequency domain.

B) Spectrum-shift

Recalling that $s_{R_i,T_n}(t)$ and $s_{R_j,T_n}(t)$ are the responses obtained at different receivers R_i, R_j, with respect to the same transmission position T_n. Denote as $\tilde{s}_{R_i,T_n}(t)$ and $\tilde{s}_{R_j,T_n}(t)$ the expressions of $s_{R_i,T_n}(t)$ and $s_{R_j,T_n}(t)$ after they pass through the down-converter of the system. Denote as $\hat{s}_{R_i,T_n}(\tau)$ and $\hat{s}_{R_j,T_n}(\tau)$ the expressions of $\tilde{s}_{R_i,T_n}(t)$ and $\tilde{s}_{R_j,T_n}(t)$ after they are projected onto the reference vector direction. Denote as $\hat{S}_{R_i,T_n}(\bar{\omega})$ and $\hat{S}_{R_j,T_n}(\bar{\omega})$ the Fourier transforms of $\hat{s}_{R_i,T_n}(\tau)$ and $\hat{s}_{R_j,T_n}(\tau)$, respectively.

According to the results given in the appendix, the relative spectrum-shift between $\hat{S}_{R_i,T_n}(\bar{\omega})$ and $\hat{S}_{R_j,T_n}(\bar{\omega})$ can be given by

$$\Omega_{j,i} = \omega_c(\gamma_{j,i} - 1) = \omega_c \frac{(\mathbf{U}_{R_j,X_o} - \mathbf{U}_{R_i,X_o})}{\mathbf{V}_{bi} \cdot \Delta\mathbf{X}}.$$

https://doi.org/10.1017/S1759078715000343 Published online by Cambridge University Press

Apparently, it does not contain the excess time-delay-related terms. By a further investigation of (6), (A.6), and (A.7), it can be seen that the excess time-delay only impact on the phase of (A.6). But, it does not impact on the relative spectrum-shift $\Omega_{j,i}$.

As discussed in the appendix, the relative spectrum-shift $\Omega_{j,i}$ can be further expressed as a function of angle-difference $(\theta_{R_j} - \theta_{R_i})$ as

$$\Omega_{j,i} \approx \omega_c \frac{\theta_{R_j} - \theta_{R_i}}{|\mathbf{V}_{bi}|\theta_{bi}},$$

where θ_{bi}, θ_{R_i} and θ_{R_j} are the angles between the normal of the target surface (i.e. vector $\mathbf{e}_3$ in Fig. 3) and the vector $\mathbf{V}_{bi}$, the projections of $\mathbf{R}_i$ and $\mathbf{R}_j$ onto the plane $\mathbf{B}$, respectively. Specially, we assume that the radar sensors (transmitter, receiver) and the target are located at the same plane (e.g. the sensors and the target are all located on the floor of a room). Then, if the normal of the target surface (i.e. vector $\mathbf{e}_3$) also locates in the same plane (e.g. in indoor environment, a wide range of objects, such as cabinets, refrigerators, etc., are with vertical surfaces. The normals of all these vertical surfaces are located in the floor plane), the angle-difference $(\theta_{R_j} - \theta_{R_i})$ given in (A.11) would be $\measuredangle R_i X_o R_j$, which is an angle-difference between the corresponding reflection directions.

In indoor environments, walls exist inevitably. It is reasonable to assume that the two sides of walls are parallel, and the rays going out the wall material can still be parallel to the incident ray (as shown in Fig. 4). Under this assumption, the angle-difference $(\theta_{R_j} - \theta_{R_i})$ does not change after the wave passing through walls. That is, the wall does not change the value of $(\theta_{R_j} - \theta_{R_i})$. Hence, the measured spectrum-shift $\Omega_{j,i}$ and the parameter $\gamma_{j,i}$ do not change after the wave passing through walls.

In short, under the given assumptions, both the excess time-delay due to walls and the refraction effect of walls do not impact on the value of spectrum-shift $\Omega_{j,i}$ and also the value of the parameter $\gamma_{j,i}$, theoretically.

C) Signal expression after data-projection

If we neglect the influence of the phase of complex reflectivity σ, it can be inferred from (A.6) that, the spectrum-shift given in (A.7) or (A.11) is same with the shift between $|\hat{S}_{R_i,T_n}(\bar{\omega}))|$ and $|\hat{S}_{R_j,T_n}(\bar{\omega}))|$. Obviously, the operation of $|\cdot|$ isolates the influence of excess time-delay incurred by walls. Let $\bar{s}_{R_i,T_n}(\tau)$ and $\bar{s}_{R_j,T_n}(\tau)$ be the inverse Fourier transform of $|\hat{S}_{R_j,T_n}(\bar{\omega}))|$ and $|\hat{S}_{R_j,T_n}(\bar{\omega}))|$, respectively. The relationship between $\bar{s}_{R_i,T_n}(\tau)$ and $\bar{s}_{R_j,T_n}(\tau)$ can be given as

$$\bar{s}_{R_j,T_n}(\tau) \approx \bar{s}_{R_i,T_n}(\tau) \exp(-j\gamma_{j,i}\tau). \tag{11}$$

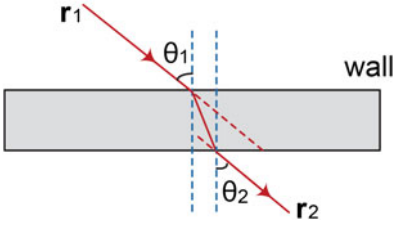

Fig. 4. The model of the wall. Assume that the rays (r_2) going out the wall material are still parallel to the incident rays (r_1). That is, $\theta_1 = \theta_2$.

If take the receiver R_1 as the reference, after the data-projection operation, we have

$$\bar{\mathbf{s}}_{T_n} = \bar{s}_{T_n}^{ref}\mathbf{K}, \tag{12}$$

where $\bar{\mathbf{s}}_{T_n} = [\bar{s}_{R_1,T_n}, \bar{s}_{R_1,T_n}, \ldots, \bar{s}_{R_M,T_n}]^T$. The superscript T indicates the transpose operation. In addition, $\bar{s}_{T_n}^{ref} = \bar{s}_{R_1,T_n}(\tau)$, and $\mathbf{K} = [1, \exp(-j\gamma_{2,1}\tau), \ldots, \exp(-j\gamma_{M,1}\tau]^T$.

For convenience of mathematical manipulation, if we consider the effects of unwanted contributions due to clutter $\mathbf{c}$ and noise $\mathbf{n}$, the signal model for all transmission positions can be given as

$$\begin{aligned}\mathbf{y} &= \bar{\mathbf{s}}^{ref} \otimes \mathbf{K} + \mathbf{c} + \mathbf{n} \\ &= \mathbf{x} + \mathbf{c} + \mathbf{n},\end{aligned} \tag{13}$$

where $\mathbf{y}$ is a $N_{MN}\times 1$ vector, $\bar{\mathbf{s}}^{ref} = [\bar{s}_{T_1}^{ref}, \bar{s}_{T_n}^{ref}, \ldots, \bar{s}_{T_N}^{ref}]^T$, and $\mathbf{x} = \bar{\mathbf{s}}^{ref} \otimes \mathbf{K}$. $N_{MN} = M \times N$, where M and N are the numbers of receivers and transmission positions, respectively. The symbol $\otimes$ denotes Kronecker product. Noise $\mathbf{n}$ and clutter $\mathbf{c}$ are $N_{MN} \times 1$ independent zero-mean complex Gaussian with known $N_{MN} \times N_{MN}$ covariance matrices $\mathbf{M}_{c+n} = E[(\mathbf{c}+\mathbf{n})(\mathbf{c}+\mathbf{n})^H]$. It is noted that $\mathbf{M}_{c+n}$ is positive semidefinite and Hermitian symmetric [7]. The superscript H indicates conjugate transpose of a matrix.

According to the CLT of the probability theory [8], if a large number of clutters from different sources (scattered from different objects) are accumulated, the statistical distribution of the sum will approach Gaussian distribution. Recalling that our scenario takes place in a cluttered indoor environment, which is with plenty of various scatterers. We assume that clutter $\mathbf{c}$ and noise $\mathbf{n}$ here could satisfy, or approach Gaussian distribution due to the "*time-delay* & *accumulation*" operations in the signal enhancement procedure. Hence, our detection problem becomes searching targets in Gaussian clutter and noise.

V. DETECTION

A) Detection problem formulation

For the detection, we define the two hypotheses:

$$H_0\text{: } \mathbf{y} = \mathbf{c} + \mathbf{n} \text{ : Clutter and noise only,}$$

$$H_1\text{: } \mathbf{y} = \mathbf{x} + \mathbf{c} + \mathbf{n} \text{ : Target plus clutter and noise.}$$

The task is to observe the return vector $\mathbf{y}$ and decide which of the two hypotheses best describes the observed vector.

Suppose $p(\mathbf{y}/H_0)$ and $p(\mathbf{y}/H_1)$ are the conditional probability density functions of the observed vector $\mathbf{y}$. The log-likelihood ratio test can be given by

$$\begin{aligned}\bar{\Lambda}(\mathbf{y}) &= \ln\frac{p(y/H_1)}{p(y/H_0)} \geq \bar{k}_{th}, \quad H_1 \text{ is true} \\ \bar{\Lambda}(\mathbf{y}) &= \ln\frac{p(y/H_1)}{p(y/H_0)}) < \bar{k}_{th}, \quad H_0 \text{ is true,}\end{aligned} \tag{14}$$

https://doi.org/10.1017/S1759078715000343 Published online by Cambridge University Press

where $\bar{k}_{th}$ is the threshold. $\bar{\Lambda}(\mathbf{y})$ can be further expressed as

$$\bar{\Lambda}(\mathbf{y}) = \ln \frac{\frac{1}{(2\pi)^{N_{MN}/2}|\mathbf{M}_{c+n}|^{1/2}} \exp\left\{-\frac{1}{2}(\mathbf{y}-\mathbf{x})^H \mathbf{M}_{c+n}^{-1}(\mathbf{y}-\mathbf{x})\right\}}{\frac{1}{(2\pi)^{N_{MN}/2}|\mathbf{M}_{c+n}|^{1/2}} \exp\left\{-\frac{1}{2}(\mathbf{y})^H \mathbf{M}_{c+n}^{-1}(\mathbf{y})\right\}} = \mathbf{x}^H \mathbf{M}_{c+n}^{-1}\mathbf{y} - \frac{1}{2}\mathbf{x}^H \mathbf{M}_{c+n}^{-1}\mathbf{x} = \Lambda(\mathbf{y}) - \frac{1}{2}\mathbf{x}^H \mathbf{M}_{c+n}^{-1}\mathbf{x}, \tag{15}$$

where $|\mathbf{M}_{c+n}|$ denotes the determinant of $\mathbf{M}_{c+n}$, and $\mathbf{M}_{c+n}^{-1}$ denotes the inverse of $\mathbf{M}_{c+n}$. Herein, the property of Hermitian symmetric matrix is used, and let

$$\Lambda(\mathbf{y}) = \mathbf{x}^H \mathbf{M}_{c+n}^{-1}\mathbf{y}. \tag{16}$$

Thus, the likelihood ratio test becomes

$$\begin{aligned} \Lambda(\mathbf{y}) &\geq k_{th}, \quad H_1 \text{ is true}, \\ \Lambda(\mathbf{y}) &< k_{th}, \quad H_0 \text{ is true}, \end{aligned} \tag{17}$$

where the threshold k_{th} is defined as

$$k_{th} = \bar{k}_{th} + \frac{1}{2}\mathbf{x}^H \mathbf{M}_{c+n}^{-1}\mathbf{x}. \tag{18}$$

B) Detector

Based on (16), (17), a detector could be given as

$$\mathbf{h} = \mathbf{M}_{c+n}^{-1}\mathbf{x} = \mathbf{M}_{c+n}^{-1}(\bar{\mathbf{s}}^{ref} \otimes \mathbf{K}).$$

In fact, it is a matched filter detector, and we have $\Lambda(\mathbf{y}) = \mathbf{h}^H\mathbf{y}$. The matrix $\mathbf{K}$ could be set based on the values of $\gamma_{j,i}$ or $\Omega_{j,i}$ given by (A.7) or (A.11).

The detector $\mathbf{h}$ can be further expressed as $\mathbf{h} = [\mathbf{h}_1, \mathbf{h}_2, ..., \mathbf{h}_N]^T$, where the element $\mathbf{h}_i \triangleq [h_{(i-1)\cdot N+1}, h_{(i-1)\cdot N+2}, \ldots, h_{(i-1)\cdot N+M}]^T$. For example, $\mathbf{h}_1 = [h_1, h_2, \ldots, h_M]^T$, $\mathbf{h}_2 = [h_{N+1}, h_{N+2}, \ldots, h_{N+M}]^T$, and so on. Similarly, we have $\mathbf{y} = [\mathbf{y}_1, \mathbf{y}_2, \ldots, \mathbf{y}_N]^T$, where the element $\mathbf{y}_i$ is defined as $\mathbf{y}_i \triangleq [y_{(i-1)\cdot N+1}, y_{(i-1)\cdot N+2}, \ldots, y_{(i-1)\cdot N+M}]^T$. Here, the symbol i in the subscript is the index of the transmission positions.

The output of the matched filter detector can be given as

$$y_{out} = \mathbf{h}^H\mathbf{y} = \sum_i^N \mathbf{h}_i^H \mathbf{y}_i. \tag{19}$$

It gives a coherent combination of signals from N-transmission positions as shown in Fig. 1. In order to lose the requirement of the phase synchronization between different transmissions, we can incoherently combine the data from different transmissions, by

$$y_{out} = \sum_i^N |\mathbf{h}_i^H \mathbf{y}_i|. \tag{20}$$

In fact, $\mathbf{h}_i^H\ \mathbf{y}_i$ in both (19) and (20) can be regarded the detection result obtained at a certain individual transmission position T_i. Then, the final output of the detector could be a coherent combination of the individual detection result $\mathbf{h}_i^H$ $\mathbf{y}_i$ as given in (19), or an incoherent combination of all the individual detection results as given in (20).

C) Threshold and performance

The probability of detection in (19), and false alarm can be given as

$$P_d = 1 - \Phi\left(\frac{k_{th} - \mathbf{h}^H\mathbf{x}}{D}\right), \tag{21}$$

$$P_f = 1 - \Phi\left(\frac{k_{th}}{D}\right), \tag{22}$$

where $\Phi(x) = \frac{1}{\sqrt{2\pi}}\int_{-\infty}^{x} e^{-t^2/2}dt$, and the parameter D is defined as

$$\begin{aligned} D^2 = \mathbf{x}^H \mathbf{M}_{c+n}^{-1}\mathbf{x} &= \frac{\mathbf{x}^H\mathbf{x}}{E[(\mathbf{y}-\mathbf{x})^H(\mathbf{y}-\mathbf{x})]} \\ &= N_{MN}\frac{x_{av}^2}{E[(\mathbf{y}-\mathbf{x})^H(\mathbf{y}-\mathbf{x})]}, \end{aligned} \tag{23}$$

where x_{av}^2 is the average signal power of $\mathbf{x}$. Generally,

$$\frac{x_{av}^2}{E[(y-x)^H(y-x)]}$$

can be regarded as the SINR at the output of the detector [9].

In terms of Neyman–Pearson criterion, the threshold k_{th} could be set as

$$k_{th} = D\Phi(1 - P_f).$$

Correspondingly, the detection probability can be further given as $P_d = 1 - \Phi(\Phi^{-1}(1 - P_f) - D)$.

VI. MEASUREMENT RESULTS

The measurement environment is shown in Fig. 5(a). A UWB M-sequence pseudo-noise radar developed by Ilmenau University of Technology in cooperation with MEODAT company [10] is used in the measurement. The sensor setup is given by Fig. 5(b). The transmitter moves along track $\mathbf{L}_l$, and illuminating the surroundings meanwhile. It is mounted on a program-controlled positioning unit (as shown in Fig. 5(a), the column-like object, which is attached on a rail mounted at the ceiling of the room). The positioning unit allows precise positioning of the transmitter antenna with 0.75 mm precision in two directions. The target is a concrete brick-like object with a square planar-surface (50 cm × 50 cm) as shown in Fig. 5. It is located at $x = 24$ cm in the track $\mathbf{L}_l$, with an orientation angle 60°. R_1–R_4 are four receivers, receiving the scattered signals from the surroundings. They are located at different directions with respect to the target. The transmitter–target–receiver angles are 13.9°, 20.3°, 26.3°, and 31.7°, respectively. The antennas of the transmitter and receivers are omnidirectional and horn antennas, respectively. As shown in Fig. 5(b), R_1 and R_2 are located in the same room with the target and the transmitter, whereas

https://doi.org/10.1017/S1759078715000343 Published online by Cambridge University Press

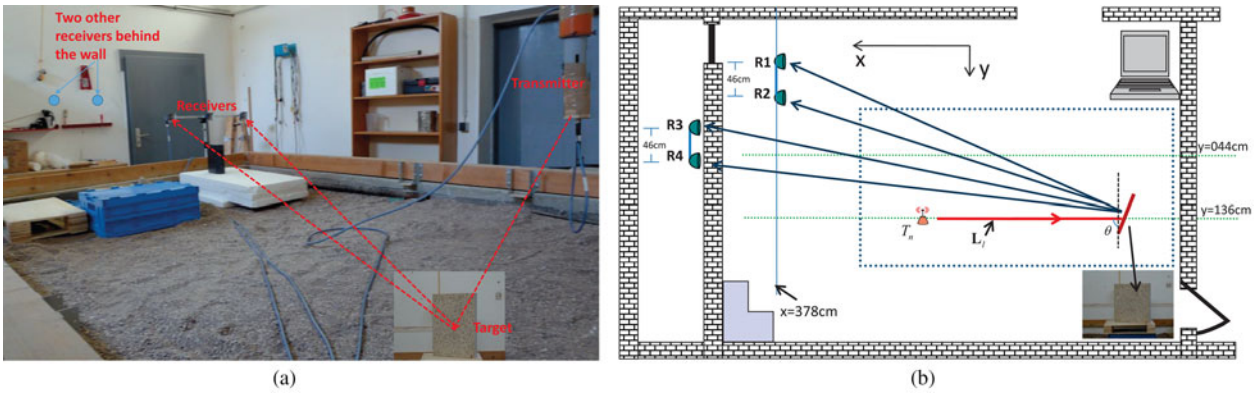

Fig. 5. Measurement setup. (a) measurement environment. The target is a concrete brick-like object with a diffuse surface. The receivers placed behind the wall are not shown in the picture. (b) Sensor setup. The target is located at $x = 24$ cm on the line L_b with an orientation angle $\theta = 60^\circ$.

R_3 and R_4 are located behind a 20-cm-thick concrete wall. Figure 6 shows the signals received by R_1–R_4. Apparently, excess time-delays exist in the signals received by R_3 and R_4. However, there is no excess time-delay for the signal received by R_1 and R_2.

In a realistic indoor environment, the response of the target is mixed with clutter and noise at the receivers. Typically, the clutter comes from objects in 3D space, such as walls, furniture, the ceiling, and also the ground, etc. Owing to the complexity of indoor environment, in a high probability, clutter is not weaker than the response of the target. In order to get a reliable detection, our first step is to enhance the responses in the line under exploration via a "*time-shift* & *accumulation*" scheme, in which the signals recorded at different transmission positions are time-shifted, aligned, and accumulated according to (5). After "*time-shift* & *accumulation*" operation, the data are projected onto the reference vector direction. This is realized by a resampling operation. Figure 7 shows the spectrum-shifts after data-projection. In the figure, $f_{R_1} \sim f_{R_4}$ are the frequencies at which the spectra have the maximum values. Theoretically, if the target presents in the scenario, for the data acquired at the true target position and orientation, the differences between f_{R_i} and f_{R_j} ($f_{R_i}, f_{R_j} \in [f_{R_1}, f_{R_2}, f_{R_3}, f_{R_4}]$) should satisfy (A.7) or (A.11). Furthermore,

$$\frac{f_{R_i} - f_{R_1}}{f_{R_j} - f_{R_1}} = \frac{\gamma_{i,1} - 1}{\gamma_{j,1} - 1} \tag{24}$$

should also be satisfied.

Figure 7(a) shows the measured result obtained at the true target position and orientation. It is shown that the results approach

$$\frac{f_{R_i} - f_{R_1}}{f_{R_j} - f_{R_1}} \approx \frac{\gamma_{i,1} - 1}{\gamma_{j,1} - 1}.$$

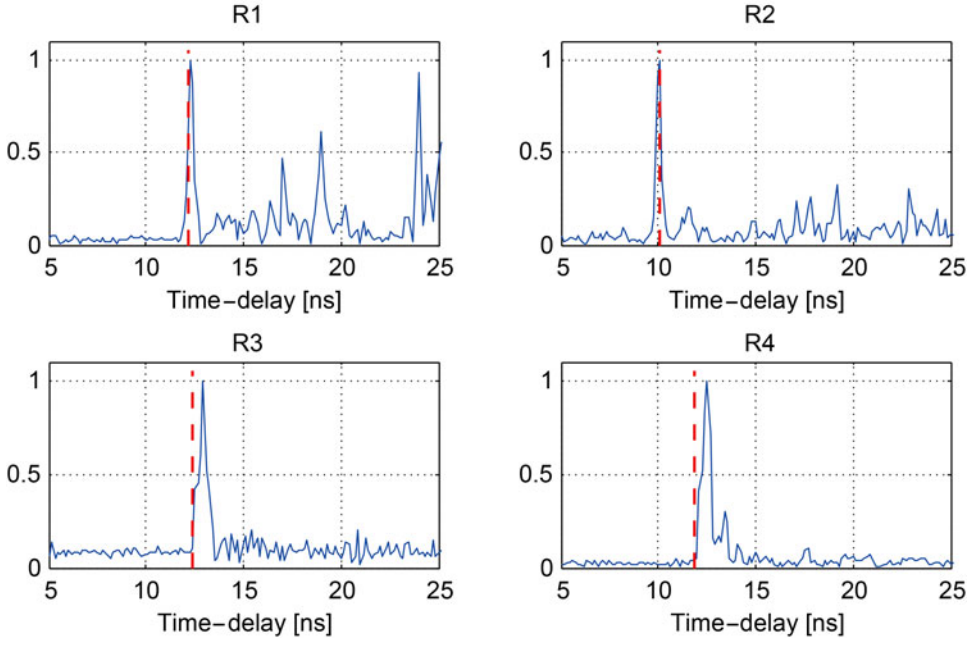

Fig. 6. Measured signals in a realistic environment given by Fig. 5(a). The red vertical line: the theoretical position of the direct-path; the first blue peak: direct-path. The vertical axis: normalized amplitude.

https://doi.org/10.1017/S1759078715000343 Published online by Cambridge University Press

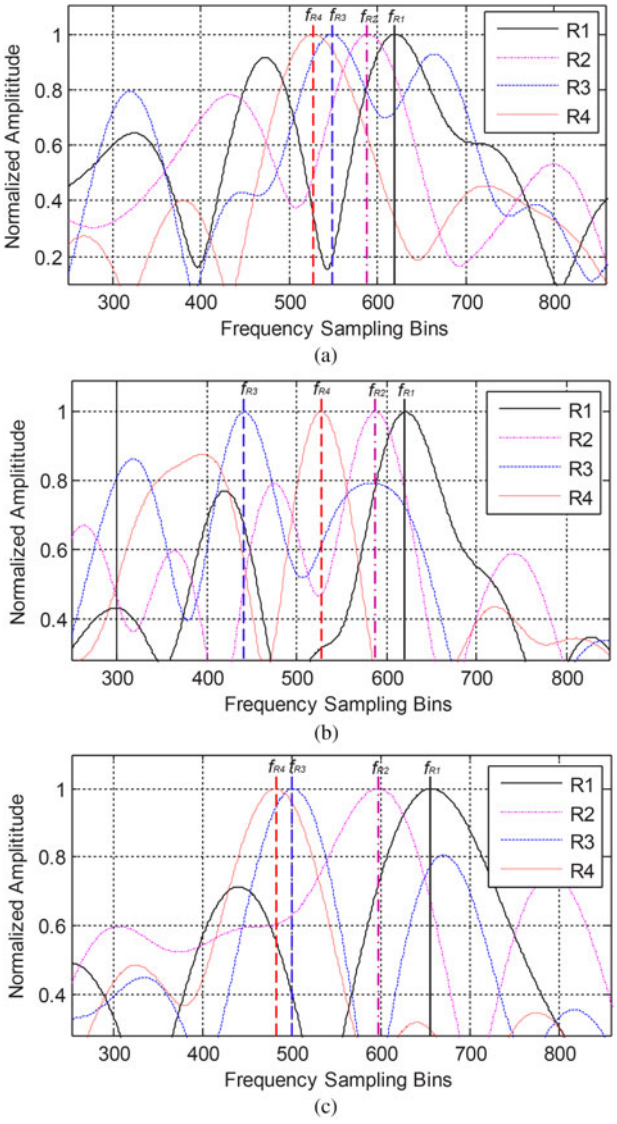

Fig. 7. Measured spectrum-shifts. (a) Spectrum-shift in a "true target position, true target orientation" condition. (b) Spectrum-shifts in a "false target position, true target orientation" condition. (c) Spectrum-shifts in a "true target position, false target orientation" condition.

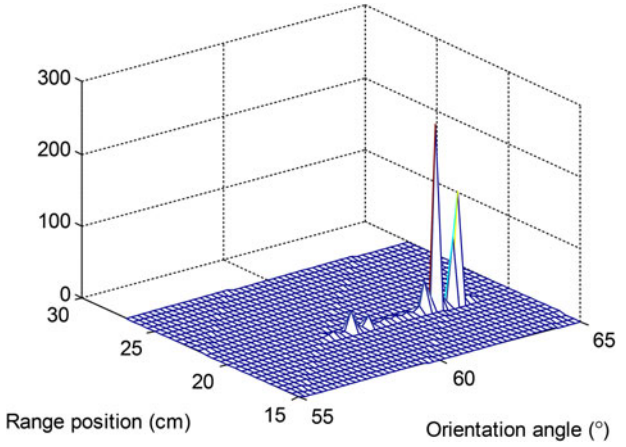

Fig. 8. The output of the detector when the transmitter locates at $x = 200$ cm.

However, Figs 7(b) and 7(c) are obtained under the condition of "false position, true orientation" and "true position, false orientation", respectively. Their results can rarely satisfy (24). As compared with (A.7) and (A.11), (24) does not demand the absolute value of ω_c, so that it is more convenient to be utilized in practice.

In Fig. 8, it shows the output of the detector when the transmitter locates at $x = 200$ cm, searching for the target position and orientation area.

In order to further fuse the detection results obtained at different transmission positions, the final detection could be a coherent/incoherent combination of these results according to (19) or (20). Figure 9(a) shows the estimates of the target position at different transmission positions. Figure 9(b) shows the estimated orientations. In the figures, the results for different data accumulation ranges, $c \cdot t^{diff}_{T_n,T'_n}$, are provided. Accumulation 1 and 2 in the figures correspond to $c \cdot t^{diff}_{T_n,T'_n} = 10$ cm and 20 cm, respectively. It is seen that their values are distributed around the true values. As indicated by the horizontal lines, the final outputs of the coherent detector are (25 cm, 61.7°) are (24.2 cm, 60.8°) for "Accumulation 1" and "Accumulation 2", respectively. The final outputs of the incoherent detector are (26 cm, 61.9°)

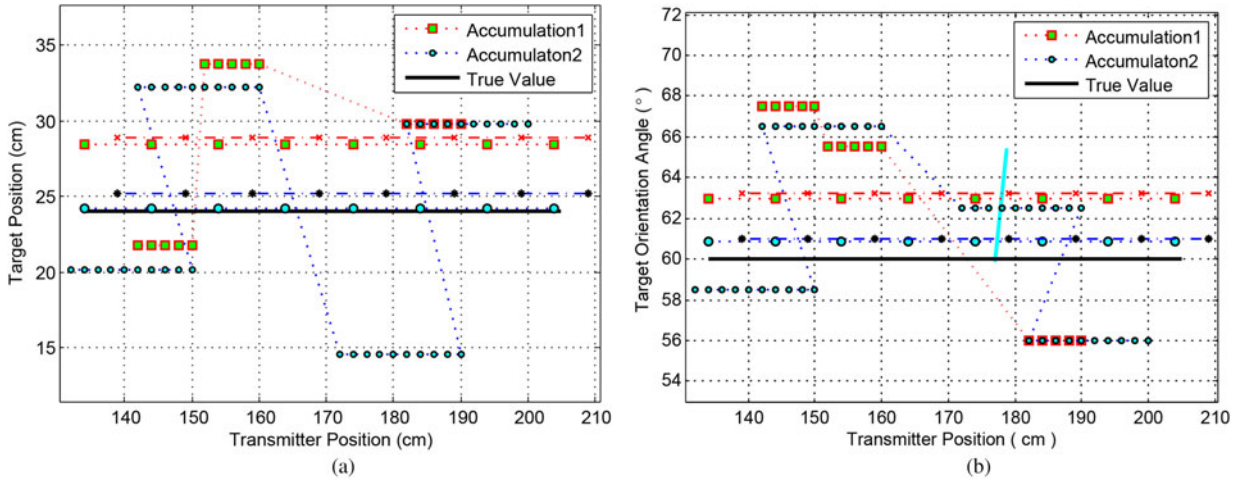

Fig. 9. Detection results. (a) Position estimates at different transmission positions. (b) Orientation estimates at different transmission positions. The ranges of "*time-shift* & *accumulation*" operation: 10 cm (Accumulation 1), 20 cm (Accumulation 2). The horizontal lines indicate the final detection results under different conditions, the "cross-dash-dot" line: "incoherent detector, accumulation 1"; The "star-dash-dot" line: "incoherent detector, accumulation 2". The other horizontal lines are the final results of the coherent detector.

https://doi.org/10.1017/S1759078715000343 Published online by Cambridge University Press

and (25.2 cm, 61.0°) for "Accumulation 1" and "Accumulation 2", respectively. It is shown that the results for "Accumulation 2" are better than "Accumulation 1" under given conditions. The results when without the data enhancement procedure is not shown in the figures, because there would be no effective results in this case.

VII. CONCLUSIONS

A stationary object detection problem in an unknown indoor environment is discussed in the paper. A "*time-shift* & *accumulation*" scheme is proposed, and a spectrum-shift-dependent detector is constructed. Using a "*time-shift* & *accumulation*" scheme, the responses of the target are time-shifted, aligned, and accumulated, while clutter from different sources is non-uniformly time-shifted and accumulated. As a consequence, the signal is enhanced, and the SINR is increased. Since the concerned target is a planar-surface object, spectrum-shift information is used to construct the detector. It is shown that this spectrum-shift information is angular-dependent, so that it is not affected by the excess time-delays incurred by walls. In fact, spectrum-shifts discussed in the paper can be regarded as a kind of angular diversity information. The property of angular diversity of a planar-surface object is distinct from other objects in the surroundings. Hence, based on this difference (or deviation), our detector is designed. In this sense, angular diversity information is used in our detector designing. In addition, the transmission positions are assumed exactly known in the paper. That is the positioning error is not considered. In our next step research, the influences of the positioning errors will be investigated, and the performance will be further evaluated under different wall parameter (e.g. thickness, orientation, material, etc.) conditions.

APPENDIX

For explanation simplicity, we suppose that the transmitted signal is an impulse signal $\delta(t)$, then after passing through the down converter, the signal which is transmitted by T_n and then received by R_i, can be expressed as

$$\tilde{s}_{R_i,T_n}(t) = \int \sigma(\mathbf{X})\delta(t - t'(\mathbf{R}_i, \mathbf{X}, \mathbf{T}_n)) \exp(-j\omega_c t) d\mathbf{X},$$

where ω_c is the central frequency of the system, $\sigma(\mathbf{X})$ is the complex reflectivity of the scatterer $\mathbf{X}$, and σ is a Gaussian distribution variable with $\sigma \sim N(0, \sigma_0^2)$. It can be further simplified as

$$\tilde{s}_{R_i,T_n}(t'(\mathbf{R}_i, \mathbf{X}, \mathbf{T}_n)) = \sigma(\mathbf{k}^{-1}(\mathbf{t})) \exp(-j\omega_c t'(\mathbf{R}_i, \mathbf{X}, \mathbf{T}_n)), \quad (A.1)$$

where $\kappa^{-1}(\cdot)$ is the inverse function of $\kappa(\cdot)$, and $\kappa(\mathbf{X}) = t'(\mathbf{R}_i, \mathbf{X}, \mathbf{T}_n)$. Using (8), the data are projected onto the reference direction defined by $\mathbf{p}_{ref}$. It can be further transformed into an expression with a new variable τ,

$$\hat{s}_{R_i,T_n}(\tau) = \sigma(\mathbf{X_o} + \mathbf{t}\mathbf{p}_{ref}/|\mathbf{p}_{ref}|^2) \exp(-j\omega_c t'(\mathbf{R}_i, \mathbf{X}_o, \mathbf{T}_n) - j\omega_c \tau). \quad (A.2)$$

The corresponding Fourier transform with respect to the variable τ can be given as

$$\hat{S}_{R_i,T_n}(\bar{\omega}) = \sigma_F(\bar{\mathbf{w}} + \mathbf{w_c}) \exp(-j\omega_c t'(\mathbf{R}_i, \mathbf{X}, \mathbf{T}_n)), \quad (A.3)$$

where $\hat{S}_{R_i,T_n}(\bar{\omega})$ and $\sigma_F(\bar{\mathbf{w}})$ are the Fourier transforms of $\hat{s}_{R_i,T_n}(\tau)$ and $\sigma(\mathbf{X_o} + \mathbf{t}\mathbf{p}_{ref}/|\mathbf{p}_{ref}|^2)$ with respect to the variable τ, respectively.

Consider the signal received by another receiver R_j, whose reception angle is different from that of R_i, as shown in Fig. 3. The time delay within the transmitter T_n, the scatterer $\mathbf{X}$, and the receiver R_j is given in (9). Similar to the analysis above, after projecting the data onto the same reference direction, the signal can be given as [11]

$$\hat{s}_{R_j,T_n}(\tau) \approx \sigma(\mathbf{X_o} + \tau\mathbf{p}_{ref}/|\mathbf{p}_{ref}|^2) \exp(-j\omega_c t'(\mathbf{R}_j, \mathbf{X_o}, \mathbf{T}_n) - j\omega_c \gamma_{j,i} \tau). \quad (A.4)$$

Similarly, in the frequency domain, it is given as

$$\hat{S}_{R_j,T_n}(\bar{\omega}) = \sigma_F(\bar{\mathbf{w}} + \mathbf{g}_{j,i}\mathbf{w_c}) \exp(-j\omega_c t'(\mathbf{R}_j, \mathbf{X_o}, \mathbf{T}_n)). \quad (A.5)$$

Statistically, it can be proofed that the cross-correlation of $\hat{S}_{R_i,T_n}(\bar{\omega})$, $\hat{S}_{R_j,T_n}(\bar{\omega})$ can be given as

$$E[\mathrm{corr}(\hat{S}_{R_i,T_n}(\bar{\omega}), \hat{S}_{R_j,T_n}(\bar{\omega}))] \approx \sigma_o^2 W(\bar{\omega} + \omega_c(\gamma_{j,i} - 1)) \cdot \exp(j\omega_c t'(\mathbf{R}_j, \mathbf{X_o}, \mathbf{T}_n) - j\omega_c t'(\mathbf{R}_i, \mathbf{X_o}, \mathbf{T}_n)), \quad (A.6)$$

where $E[\cdot]$ is a mathematical expectation operator, $\mathrm{corr}(\cdot,\cdot)$ is a cross-correlation operator. σ_o^2 is the variance of the reflectivity of scatterers. $W(\cdot)$ is the output of the correlation operation between the windows functions determined by the frequency range of the spectrum. Constant amplitude is omitted in (A.7). This result is firstly proofed and testified by *C.Prati* and *F.Rocca* in a spaceborne radar imaging scenario [11].

According to (A.6), apparently, $\omega_c(\gamma_{j,i} - 1)$ is the relative spectrum shift between $\hat{S}_{R_i,T_n}(\bar{\omega})$ and $\hat{S}_{R_j,T_n}(\bar{\omega})$. According to (10), the relative spectrum shift can be further expressed as

$$\Omega_{j,i} = \omega_c(\gamma_{j,i} - 1) = \omega_c \frac{(\mathbf{U}_{R_j,X_o} - \mathbf{U}_{R_i,X_o})}{\mathbf{V}_{bi} \cdot \Delta\mathbf{X}}. \quad (A.7)$$

As shown in Fig. 3, the symbol $\mathbf{A}$ stands for the target-surface plane. $\mathbf{e}_1$ is the unit vector of the projection of $\mathbf{V}_{bi}$ on the target-surface plane. We define another two unit vectors $\mathbf{e}_2$, $\mathbf{e}_3$ as

$$\mathbf{e}_2 = \frac{\mathbf{e}_1 \times \mathbf{V}_{bi}}{|\mathbf{e}_1 \times \mathbf{V}_{bi}|}, \quad \mathbf{e}_3 = \frac{\mathbf{e}_1 \times \mathbf{e}_2}{|\mathbf{e}_1 \times \mathbf{e}_2|}, \quad (A.8)$$

where " × " denotes "cross product" or vector product. If we regard the unit vectors $\mathbf{e}_1$, $\mathbf{e}_2$, $\mathbf{e}_3$ as a set of basis vectors, $\{\mathbf{e}_1, \mathbf{e}_2, \mathbf{e}_3\}$ would span a 3D space R^3, in which $\{\mathbf{e}_1, \mathbf{e}_2\}$ spans the target-surface plane $\mathbf{A}$. Apparently, $\mathbf{e}_3$ is located in the normal direction of the plane $\mathbf{A}$, and we have $\mathbf{e}_1 \cdot \mathbf{e}_2 = \mathbf{V}_{bi} \cdot \mathbf{e}_2 = 0$.

https://doi.org/10.1017/S1759078715000343 Published online by Cambridge University Press

As shown in Fig. 3, $\Delta\mathbf{X}$ is a vector locating on the target-surface plane A. It can be decomposed as

$$\Delta\mathbf{X} = x_{e1}\mathbf{e}_1 + x_{e2}\mathbf{e}_2. \tag{A.9}$$

In (A.7), the value of $(\mathbf{U}_{R_j,X_o} - \mathbf{U}_{R_i,X_o})$ depends on the relative position of the vectors $\mathbf{R}_i$ and $\mathbf{R}_j$. If we adjust the relative positions of $\mathbf{R}_i$ and $\mathbf{R}_j$, so as to let $(\mathbf{U}_{R_j,X_o} - \mathbf{U}_{R_i,X_o}) \cdot \mathbf{e}_2 = 0$ is satisfied. Thus, we have

$$(\mathbf{U}_{R_j,X_o} - \mathbf{U}_{R_i,X_o}) \cdot (\mathbf{e}_1 \times \mathbf{V}_{bi}) = 0. \tag{A.10}$$

It implies that the vector $(\mathbf{U}_{R_j,X_o} - \mathbf{U}_{R_i,X_o})$ is parallel to the plane $\mathbf{B}$, which is spanned by $\{\mathbf{e}_1, \mathbf{e}_3\}$ or $\{\mathbf{e}_1, \mathbf{V}_{bi}\}$, as shown in Fig. 3.

Let $\tilde{\mathbf{U}}_{R_i,X_o}$ and $\tilde{\mathbf{U}}_{R_j,X_o}$ denote the projections of $\mathbf{U}_{R_i,X_o}$ and $\mathbf{U}_{R_j,X_o}$ on the plane $\mathbf{B}$, respectively. And θ_{R_i}, θ_{R_j} are the angles formed by the vector $\tilde{\mathbf{U}}_{R_i,X_o}$ and $\mathbf{e}_3$, $\tilde{\mathbf{U}}_{R_j,X_o}$ and $\mathbf{e}_3$, respectively. That is, θ_{R_i} and θ_{R_j} are, respectively, the reflection angles of the projections of and $\mathbf{R}_j$ onto the plane $\mathbf{B}$. Apparently, $\sin\theta_{R_j} = \tilde{\mathbf{U}}_{R_j,X_o} \cdot \mathbf{e}_1$, $\sin\theta_{R_i} = \tilde{\mathbf{U}}_{R_i,X_o} \cdot \mathbf{e}_1$. Hence, after some calculations, (A.7) can be further simplified as

$$\Omega_{j,i} = \omega_c(\gamma_{j,i} - 1) = \omega_c \frac{\sin\theta_{R_j} - \sin\theta_{R_i}}{|\mathbf{V}_{bi}|\sin\theta_{bi}} \approx \omega_c \frac{\theta_{R_j} - \theta_{R_i}}{|\mathbf{V}_{bi}|\theta_{bi}}, \tag{A.11}$$

where θ_{bi} is the angle between the vector $\mathbf{V}_{bi}$ and $\mathbf{e}_3$.

REFERENCES

[1] Scheer, W.L.M.J.A. (ed.): Principles of Modern Radar, vol. III of Radar Applications, SciTech Publishing, an imprint of the IET, Edison, NJ, 2014.

[2] Moura, J.M.F.; Jin, Y.: Time reversal imaging by adaptive interference canceling. IEEE Trans. Signal Process., **56** (1) (2008), 233–247.

[3] Varslot, T.; Yazici, B.; Yarman, C.-E.; Cheney, M.; Scharf, L.: Time-reversal waveform preconditioning for clutter rejection, in Proc. Int. Waveform Diversity and Design Conf., 2007, 330–334.

[4] Borcea, L.; Papanicolaou, G.; Tsogka, C.; Berryman, J.: Imaging and time reversal in random media. Inverse Probl., **18** (2002), 1247.

[5] Zhang, W.; Hoorfar, A.; Li, L.: Through-the-wall target localization with time reversal music method. Progress Electromagn. Res., **106** (2010), 75–89.

[6] Wang, L.J.Z.H.F.: Experimental investigation of selective localization by decomposition of the time reversal operator and subspace-based technique. IET Radar, Sonar Navig., **2** (6) (2008), 426–434.

[7] van den Bos, A.: The multivariate complex normal distribution-a generalization. IEEE Trans. Inf. Theory, **41** (2) (1995), 537–539.

[8] Kobayashi, H.; Mark, B.L.; Turin, W.: Probability, Random Processes, and Statistical Analysis, Cambridge University Press, Cambridge, UK, 2012.

[9] Poor, H.V.: An Introduction to Signal Detection and Estimation, Chapter III, 2nd ed., Springer-Verlag, New York, 1994.

[10] Zetik, R.; Sachs, J.; Thoma, R.S.: Uwb short-range radar sensing – the architecture of a baseband, pseudo-noise UWB radar sensor. IEEE Instrum. Meas. Mag., **10** (2) (2007), 39–45.

[11] Prati, C.; Rocca, F.: Improving slant-range resolution with multiple SAR surveys. IEEE Trans. Aerosp. Electron. Syst., **29** (1) (1993), 135–143.

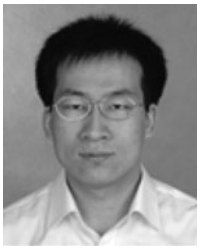

Honghui Yan received his B. Sc. degree in Information & Communication Engineering from Shanxi University, Taiyuan, China, in 1997 and M. Sc. degree from Armored Force Engineering College, Beijing, China, in 2002 and Ph. D. degree from the Institute of Electronics, Chinese Academy of Sciences (IECAS), Beijing, China, in 2005. From 2005 to 2008, he was a Research Associate with the airborne radar R&D Department of IECAS, where he conducted research in the field of Synthetic Aperture Radar (SAR) signal processing, bi/multistatic radar theory, as well as SAR interferometry. And then he worked in the field of UWB radar system with the Electronic Measurement Research Laboratory (EMT) at Ilmenau University of Technology, Germany. Currently, he is working for MIMO radar in Sony EuTEC. His research interests include Radar Imaging and Detection, Localization and Tracking, MIMO Radar, as well as Digital Signal Processing.

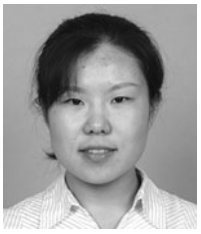

Qiaozhen Liu received her Ph.D degree at BeiHang University in 2005. Currently she is working for Beijing Institute of Astronautical Systems Engineering. She is a professor in the field of signal processing and astronautical system design.

Prof. Dr.-Ing. R. Thomä received the Dipl.-Ing. (M.S.E.E.), Dr.-Ing. (Ph.D.E.E.), and the Dr.-Ing. habil. degrees in electrical engineering and information technology from Technische Hochschule Ilmenau, Germany, in 1975, 1983, and 1989, respectively.

From 1975 to 1988, he was a Research Associate in the fields of electronic circuits, measurement engineering, and digital signal processing at the same university. From 1988 to 1990, he was a Research Engineer at the Akademie der Wissenschaften der DDR (Zentrum für Wissenschaftlichen Gerätebau). During this period, he was working in the field of radio surveillance. In 1991, he spent a three-month sabbatical leave at the University of Erlangen-Nürnberg (Lehrstuhl für Nachrichtentechnik). Since 1992, he has been a Professor of electrical engineering (electronic measurement) at TU Ilmenau where he was the Director of the Institute of Communications and Measurement Engineering from 1999 until 2005. With his group, he has contributed to many European and German research projects and clusters such as WINNER, PULSERS, EUWB, NEWCOM, COST 273, 2100, EASY-A, EASY-C. Currently he is the speaker of the German nation-wide DFG-focus project UKoLOS, Ultra-Wideband Radio Technologies for Communications, Localization and Sensor Applications (SPP 1202). Since 1999 he has been serving as chair of the

https://doi.org/10.1017/S1759078715000343 Published online by Cambridge University Press

IEEE-IM TC-13 on Measurement in Wireless and Telecommunications. In 2007 he was awarded IEEE Fellow Member and received the Thuringian State Research Award for Applied Research both for contributions to high-resolution multidimensional channel sounding. His research interests include measurement and digital signal processing methods (correlation and spectral analysis, system identification, array methods, time-frequency and cyclostationary signal analysis), their application in mobile radio and radar systems (multidimensional channel sounding, propagation measurement and parameter estimation, ultra-wideband radar), measurement-based performance evaluation of MIMO transmission systems, and UWB sensor systems for object detection and imaging.

https://doi.org/10.1017/S1759078715000343 Published online by Cambridge University Press